NeuroImage: Clinical 14 (2017) 363–370

Contents lists available at ScienceDirect

NeuroImage: Clinical

journal homepage: www.elsevier.com/locate/ynicl

New rapid, accurate T_2 quantification detects pathology in normal-appearing brain regions of relapsing-remitting MS patients

Timothy M. Shepherd[a,b], Ivan I. Kirov[a,b], Erik Charlson[c], Mary Bruno[a], James Babb[a], Daniel K. Sodickson[a,b], Noam Ben-Eliezer[a,b,*]

[a]Department of Radiology, New York University Langone School of Medicine, New York, NY, United States
[b]Center for Advanced Imaging Innovation and Research (CAI2R), New York, NY, United States
[c]Department of Neurology & Multiple Sclerosis Comprehensive Care Center, New York University Langone School of Medicine, New York, NY, United States

ARTICLE INFO

Article history:
Received 27 September 2016
Received in revised form 18 January 2017
Accepted 25 January 2017
Available online 3 February 2017

Keywords:
Relaxation
Mesoscopic
Demyelination
Neurodegeneration
Biomarkers

ABSTRACT

Introduction: Quantitative T_2 mapping may provide an objective biomarker for occult nervous tissue pathology in relapsing-remitting multiple sclerosis (RRMS). We applied a novel echo modulation curve (EMC) algorithm to identify T_2 changes in normal-appearing brain regions of subjects with RRMS (N = 27) compared to age-matched controls (N = 38).
Methods: The EMC algorithm uses Bloch simulations to model T_2 decay curves in multi-spin-echo MRI sequences, independent of scanner, and scan-settings. T_2 values were extracted from normal-appearing white and gray matter brain regions using both expert manual regions-of-interest and user-independent FreeSurfer segmentation.
Results: Compared to conventional exponential T_2 modeling, EMC fitting provided more accurate estimations of T_2 with less variance across scans, MRI systems, and healthy individuals. Thalamic T_2 was increased 8.5% in RRMS subjects ($p < 0.001$) and could be used to discriminate RRMS from healthy controls well (AUC = 0.913). Manual segmentation detected both statistically significant increases (corpus callosum & temporal stem) and decreases (posterior limb internal capsule) in T_2 associated with RRMS diagnosis (all $p < 0.05$). In healthy controls, we also observed statistically significant T_2 differences for different white and gray matter structures.
Conclusions: The EMC algorithm precisely characterizes T_2 values, and is able to detect subtle T_2 changes in normal-appearing brain regions of RRMS patients. These presumably capture both axon and myelin changes from inflammation and neurodegeneration. Further, T_2 variations between different brain regions of healthy controls may correlate with distinct nervous tissue environments that differ from one another at a mesoscopic length-scale.

1. Introduction

Relapsing-remitting multiple sclerosis (RRMS) is a common neurological disease affecting young adults and characterized by recurrent clinically-symptomatic episodes of inflammation and the insidious progression of disability. The classic MRI hallmarks for RRMS are transient foci of contrast enhancement during acute inflammatory episodes and the gradual accumulation of T_2 or FLAIR hyperintensities. Previous studies have established that foci of T_2 prolongation correlate with inflammation, edema, demyelination, abnormal re-myelination, gliosis and/or axonal loss (Laule et al., 2011, 2013; Lund et al., 2012; MacKay et al., 2006). Although not all T_2-bright lesions are MS-related (Liu et al., 2013), the number and locations of focal T_2 hyperintensities can often help support the clinical diagnosis of MS (Polman et al., 2010). However, T_2 changes from subtle tissue pathology can be hard to detect visually on clinical MRI scans particularly during early stages of the disease. Further, visually-apparent T_2 lesions correlate poorly with patient disability or MS disease progression (Barkhof, 2002).

This radiology-pathology discordance in MS patients has been attributed to inflammation and neurodegeneration that remain occult to visible detection on conventional MRI. Several advanced techniques, such as MR spectroscopy, diffusion, and magnetization transfer MRI, have demonstrated abnormalities in normal-appearing brain regions for MS patients (Ceccarelli et al., 2007; Davie et al., 1997; Mangia et al., 2014). Subtle T_2 differences have also been observed in normal-appearing white matter as well (Bonnier et al., 2014; Laule et al., 2004). While each of these techniques may have clinical value for the

Abbreviations: AUC, area under the curve; B1+, transmit field; EMC, echo modulation curve; FLAIR, fluid-attenuated inversion recovery; SPACE, sampling perfection with application-optimized contrasts using different flip angle evolution; MPRAGE, magnetization-prepared rapid gradient-echo; SSE, single spin echo; MSE, multi-spin echo; MWF, myelin water fraction; ROI, Region of Interest; RRMS, relapsing-remitting multiple sclerosis; WM, white matter; GM, gray matter.

* Corresponding author at: Department of Radiology, 4th floor, No. 401, 660 First Ave., New York, NY 10016, United States.
E-mail address: Noam.BenEliezer@nyumc.org (N. Ben-Eliezer).

http://dx.doi.org/10.1016/j.nicl.2017.01.029

early diagnosis of MS and monitoring disease progression, quantitative methods also may provide more objective markers of specific pathological components of MS. However, to realize this potential, these methods need to be accurate, stable and reproducible across different MRI protocols and imaging sites – features that remain elusive for diffusion, magnetization transfer and conventional T_2 mapping techniques.

Accurate T_2 mapping in *clinically-feasible* scan times is challenging due to the inherent bias of rapid multi spin-echo (MSE) sequences by stimulated and indirect echoes, non-rectangular slice profiles and transmit-field (B_1^+) inhomogeneities. Furthermore, this bias depends on the pulse sequence implementation and scan parameters, causing T_2 values in the same subject to vary between scanners and protocols (Deoni et al., 2003; Lebel and Wilman, 2010; Poon and Henkelman, 1992). T_2 estimation accuracy may be improved with short TR single spin echo (SSE) (Sussman et al., 2010), analytical solutions to coherence pathways in MSE acquisitions (Lebel and Wilman, 2010; Lukzen et al., 2009; Prasloski et al., 2012), model-based reconstruction approaches (Huang et al., 2012), modeling signal with non-spin echo based pulse sequences (Deoni et al., 2003; Schmitt et al., 2004; Warntjes et al., 2007), or heuristic signal model approaches (Ma et al., 2013). We have recently reported an alternative approach for accurate quantitative T_2 mapping, the echo modulation curve (EMC) algorithm, which uses a Bloch simulation to trace all coherence pathways, including all stimulated and indirect echoes during an MSE acquisition. This algorithm accounts for different slice profiles, radiofrequency pulse shapes, crusher gradients, and spin relaxation during the radiofrequency (RF) pulses (Ben-Eliezer et al., 2015a). Because the EMC algorithm incorporates the specific implementation of the MSE pulse-sequence, this method is robust to different acquisition strategies, and offers reliable mapping in clinically feasible scan times. Note that acquisitions for EMC fitting can be tailored to emphasize speed and/or accuracy for particular T_2 components. Further info can be found in a recent report including detailed analysis of T_2 mapping approaches, and demonstrating the advantage of Bloch-simulation-based approach, like EMC, over extended phase-graph (EPG) techniques (McPhee and Wilman, 2016).

Here, we used the EMC algorithm to characterize different brain regions in a cohort of clinical RRMS patients compared to healthy age-matched controls. Using this technique we were able to detect subtle, yet statistically significant, anatomy-specific T_2 differences within normal-appearing gray and white matter structures in RRMS patients. We also observed interesting T_2 differences in healthy control subjects between individual brain structures with different anatomic locations or specific functions.

2. Materials & methods

2.1. Subject enrollment & MRI protocol

This study was performed with approval from the local institutional review board. The MSE sequence was part of the routine noncontrast head protocol for patients with an established clinical diagnosis of multiple sclerosis, referred from our academic center's MS neurology specialists and scheduled on an outpatient 3-T MRI scanner with a 20-channel head & neck coil (Skyra or Prisma, Siemens Healthcare, Erlangen, Germany). MSE scan parameters were: TR = 2500 ms, Echo-spacing = 12 ms, First echo-time = 12 ms, N_{echoes} = 10, res = 1.7 × 1.7 mm^2, N_{slices} = 23, slice-thickness = 3 mm, bandwidth = 200 [Hz/Px], $T_{acquisition}$ = 2:44 min using 2× GRAPPA acceleration. The use of longer echo trains could theoretically improve T_2 fitting accuracy (Whittall et al., 1997), particularly if long T_2 components contribute to voxel signal (e.g. in more cystic MS lesions). These are not the focus of the current work and investigation of such tissues is left for future study. However, the specific absorption rate (SAR) and scan-time limitations when scanning patients in clinical settings, limited the number of echoes that could be used while keeping sufficient volumetric coverage (i.e., number of sliced). Also note that since intravenous contrast was not ordered in these subjects, the ordering clinician's suspicion for active inflammatory lesions was low. The standard MRI protocol also included sagittal 3D SPACE FLAIR, axial susceptibility-weighted imaging, and a 3D 1-mm isotropic volumetric MPRAGE sequence. A board-certified neuroradiologist confirmed typical MRI findings consistent with clinical MS (Polman et al., 2010). A board-certified neurologist reviewed the electronic medical record to confirm MS diagnosis and subtype, disease duration and the most recent documented patient-reported expanded disability scale score (PDSS) (Hohol et al., 1995). PDSS is similar, and correlates strongly, with the expanded disability status scale (EDSS) (Learmonth et al., 2013). PDSS, however, is more efficient to collect in routine clinical care. A PDSS score of "1" indicates mild disability, "2" indicates moderate disability without gait impairment, "3" reflects gait impairment without use of a cane, and "4–5" indicate early use of a cane (after 25 ft of walking) vs late use of cane (required to walk even 25 ft). During this chart review, 2 subjects with secondary progressive MS and 1 subject with primary progressive MS were identified and excluded from the study. Overall, 27 subjects with RRMS (19 females, mean age 48.5 ± 9.2 years/o) with mean disease duration of 12.6 ± 8.6 years and PDSS of 2 ± 1.8 (no units) were included in this study. A PDSS of 2 corresponds to significant problems related to MS such as visual impairment, sensory symptoms, or fatigue, but no limitations in walking ability. Age-matched control subjects (N = 38, 15 females, mean age 39.0 ± 9.6 years/o) without history of neurological disease or known white matter hyperintensities were recruited from the local community.

2.2. T_2 relaxation mapping

T_2 maps were generated via (a) pixel-by-pixel fitting of the MSE time series of DICOM images to a theoretical exponential decay of the form of $S(t) = S_0 \cdot e^{-t/T_2}$ (Levitt, 2001) and (b) using the EMC algorithm (Ben-Eliezer et al., 2015a). All fitting procedures were programmed in-house using C++ and MATLAB (The MathWorks Inc., Natick, MA). The EMC algorithm consists of an initial pre-processing stage, in which Bloch simulations of the prospective MSE protocol are performed using the exact RF pulse shapes and other parameter values used on the MRI scanner. This allows EMC to replicate the actual decay curve in MSE protocols and produce T_2 values that are independent of the particular choice of experimental parameter set. Simulations are repeated for a range of T_2 relaxation values and transmit-field (B_1^+) inhomogeneity levels (T_2 = 1 … 1000 ms, B_1^+ = 70 … 130%), producing a database of decay curves each associated with a unique [B_1^+, T_2] value pair. Once experimental MSE data are acquired, the signal time series from each pixel is matched to the simulated database of EMCs by calculating the L2 norm of the difference between the experimental and simulated decay curves, and choosing the database entry that yields the minimum norm. This minimization procedure is implemented using a full search over the entire database, which is completed in ~15 s per slice. A unique T_2 value associated with the matched EMC is then assigned to the corresponding pixel, eventually yielding the desired parametric map after the procedure is repeated for all pixels in the slice. To avoid fitting bias due to Rician noise, signal decay curves are truncated below 10% of the first time-point intensity – for both exponential and EMC fitting. This resulted in exclusion of 1–2 echoes in areas of very short T_2 values. Lastly, proton density (PD) maps are calculated by extrapolating the image from the first echo time to time t = 0 s based on the calculated T_2 map under the assumption that purely exponential decay takes place between spin excitation and the first acquisition event.

2.3. Region of Interest (ROI) analysis

Volumetric segmentation of six ROIs was performed using automated FreeSurfer software (http://surfer.nmr.mgh.harvard.edu/) based on the three-dimensional T_1-weighted MPRAGE data. The ROIs included: global white matter, cortical gray matter, thalamus, caudate nucleus,

putamen and globus pallidus. ROIs were then delineated on the T_2 maps by co-registering these maps to FreeSurfer atlas space using FreeSurfer conversion and registration tools. Lastly, the perimeter of these automated ROIs was eroded by one pixel in order to avoid edge artifact such as partial volume effects.

Manual ROIs were drawn by a board-certified neuroradiologist on 5 different axial T_2-weighted images (A-E) with TE = 81 ms, similar to standard clinical T_2-weighting (Fig. 1). At slice A, 6 ROIs were drawn for the bilateral optic radiations, temporal stem white matter and globus pallidus. At slice B, 8 ROIs were drawn for the bilateral caudate nucleus, putamen, thalamus and posterior limb internal capsule. At slice C, 2 ROIs were drawn for the genu and splenium of the corpus callosum. At slice D, a single ROI was drawn for the body of the corpus callosum. At slice E, 2 ROIs were drawn for the bilateral centrum semiovale. As an internal control, additional smaller ROIs were drawn within T_2-bright lesions located in the periventricular, subcortical and juxtacortical white matter for each of the RRMS subjects and compared to similarly located ROIs in healthy controls (see Fig. 2). For all other ROIs, T_2-bright lesions were avoided. In some cases this meant no data could be obtained for specific ROIs in individual RRMS subjects.

Analysis of covariance (ANCOVA) was used to compare controls and RRMS subjects for the mean T_2 value in each ROI adjusted for both age and sex. The error variance was allowed to differ across comparison groups to remove the assumption of variance homogeneity. Logistic regression and area under the ROC curve (AUC) was used to assess the utility of each measure to discriminate patients with and without lesions. Pearson correlation coefficients were used to assess the relationship between ROI T_2 values and disease duration (years) and the ordinal PDSS. All statistical tests were conducted with SPSS 22 (IBM, Armonk, NY) at the two-sided 5% significance level. The purpose of this study was to identify potential T_2 differences from many different brain regions so corrections for multiple comparisons was not conducted a priori – this may increase the risk of Type 1 errors but reduces the chance of detecting small T_2 differences for investigation for future studies.

3. Results

3.1. Exponential and EMC T_2 fitting comparison

Table 1 presents comparison of exponential and EMC fitting for 5 representative brain regions, and across all 38 healthy control subjects. Values demonstrate an average increase of 59% in mean T_2 and 108% larger standard deviation for exponential fitting compared to EMC fitting ($p < 0.001$, all 5 regions). The EMC T_2 values are very similar to previously published T_2 values for these regions, when compared against a reference single spin echo (SSE) based T_2 values (Ben-Eliezer et al., 2015a, 2016). SSE scans, however, require 50 min or more per scan and would not be practical in this larger study, especially for RRMS patients. Given these findings, we focus solely on EMC analysis for the remainder of this report.

3.2. Baseline and RRMS-specific differences in brain T_2

In the FreeSurfer ROI analysis (Fig. 3) statistically significant increases were observed for most deep gray matter structures, with the largest observed difference being an 8.5% increase in thalamus T_2 for RRMS subjects. Age did not affect thalamic T_2 in control subjects and showed only a very weak positive correlation in RRMS subjects ($R = 0.0154$, $p < 0.0001$) (Fig. 4) . An ROI of global white matter that excluded regions of T_1 hypointensity did not detect significant T_2 differences between the groups. Conversely, the manual ROI analysis demonstrated several normal-appearing white matter regions with either statistically increased (temporal stem, body and genu corpus callosum) or decreased T_2 values (posterior limb internal capsule) (Table 2). Potential explanations for the differences between FreeSurfer and manual ROI analyses are discussed below. It should also be noted that for all normal-appearing brain regions the intra-ROI SD – which reflects T_2 (and general) tissue heterogeneity – was consistently higher in the RRMS patients, for both FreeSurfer and manual segmentations. Manual ROIs purposefully drawn in juxtacortical, subcortical and periventricular white matter lesions (obvious to a neuroradiologist on the T_2-weighted reconstructed images) demonstrated 35.5–39.1% T_2 increases compared to homologous regions in healthy controls (all comparisons, $p < 0.001$). We also observed statistically significant T_2 differences between multiple gray and white matter regions in healthy controls (Table 2 and Fig. 5). Analysis of the manually segmented ROI demonstrated no significant left-right T_2 differences for controls or RRMS patients.

3.3. Potential diagnostic utility of EMC T_2 maps

We also tested the hypothesis that T_2 values in brain regions without T_2-bright lesions might be used to discriminate between controls and RRMS subjects. The FreeSurfer-segmented whole-thalamus ROI was found to be an excellent discriminator between the two groups (AUC = 0.913) – this accuracy left insufficient room for improvement

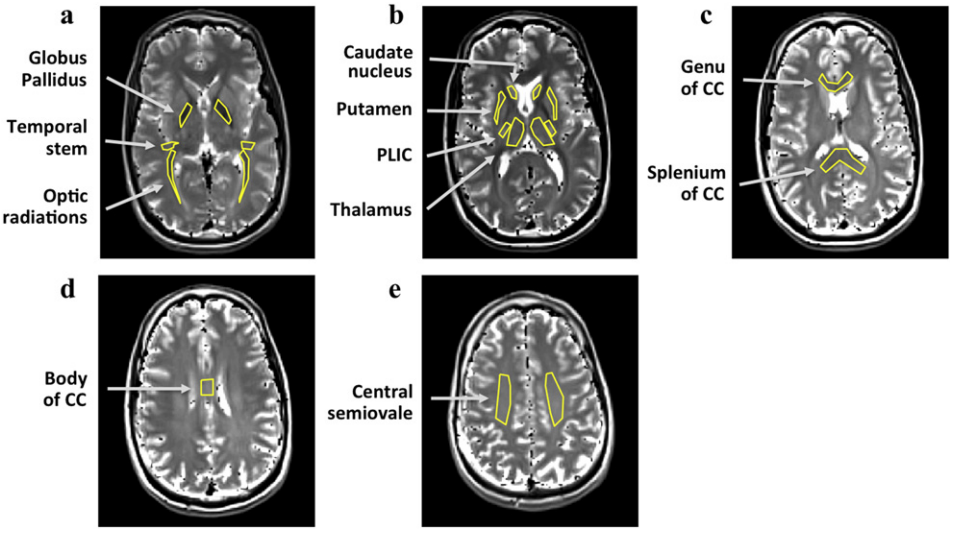

Fig. 1. Expert-drawn manual regions-of-interest for a single subject with relapsing-remitting multiple sclerosis. 5 axial slices were included for the analysis; immediately below the anterior commissure (a), at the foramen of Monro (b), 1 cm above the foramen of Monro (c), roof of the lateral ventricles (d) and 1 cm above the lateral ventricles (e).

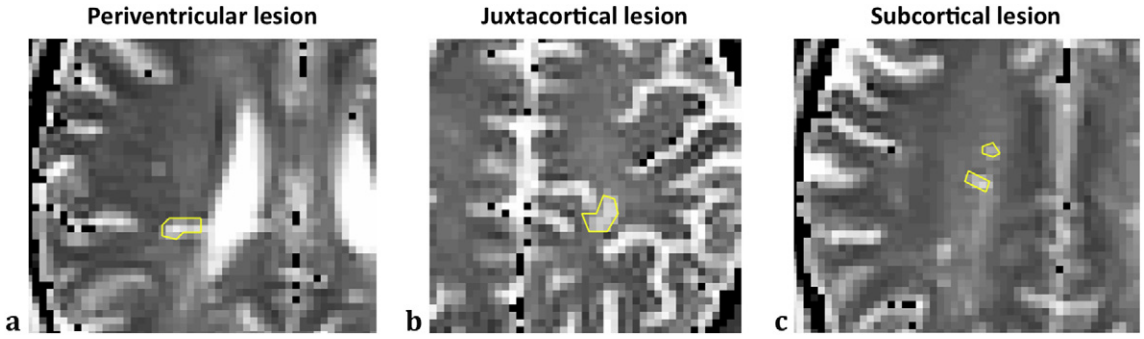

Fig. 2. Examples of regions-of-interest for MS lesions including (a) periventricular, (b) juxtacortical and (c) subcortical white matter. ROIs were drawn on a T_2 weighted image (TE = 81 ms) synthesized based on EMC fitted T_2 map without interpolation (note, black voxels indicate non-valid fitting results). Similar ROIs were drawn for investigating normal appearing brain regions, i.e., where lesions were not visibly present to a board-certified neuroradiologist (see Fig. 1).

by the addition of a second regional T_2 measure to the diagnostic model. Another secondary aim of this retrospective study was to determine whether T_2 values in individual brain regions, correlated with readily available clinical information in the electronic medical record for RRMS subjects. There was a modest negative correlation between RRMS disease duration, and the T_2 values in normal-appearing juxtacortical white matter ($r = -0.46$, $p = 0.017$). We also observed statistical trends ($p < 0.1$) for correlations between RRMS disease duration and subcortical white matter lesion and thalamic T_2 increases. We did not observe regional T_2 correlations to patient-reported disability scale score (PDSS).

4. Discussion

4.1. T_2 changes in RRMS

Automated segmentation using FreeSurfer detected a statistically significant 8.5% increase in the thalamus T_2 ($p < 0.001$). The thalamus can be affected early in the natural history of MS as a result of demyelination, iron accumulation, and axonal and synaptic loss (Gilmore et al., 2009). The thalamus is a major relay station within the nervous system such that the observed MS-related thalamic T_2 changes may also reflect sequelae of retrograde degeneration from its widespread cortical and subcortical connections. Thalamic neuropathological changes and volume loss correlate with clinical symptoms of fatigue, dystonia, memory impairment and decreased processing speed (Minagar et al., 2013). Additional statistically significant T_2 increases were observed with automated analysis for other gray matter structures, including cortex, pallidum and putamen (Fig. 2). Previous studies reported *decreased* T_2-weighted image intensity (and hence inferred shorter T_2 and T_2^*) in the caudate nucleus, putamen, globus pallidus and thalamus for clinically-isolated syndrome and MS patients. These differences progressed over time in individual subjects and were attributed to microscopic iron accumulation (Khalil et al., 2009). The current results may differ since, compared to signal intensity variations on T_2-weighted images in previous reports, the multi spin-echo data used by the EMC algorithm is less sensitive to diffusion-mediated T_2^* signal attenuation.

Manual ROIs within gray matter regions did not detect statistical differences between RRMS subjects and healthy controls. There are 3 potential explanations for this discordance. First, the automated method holds higher statistical power by including the entire structure volume, whereas manual segmentation delineated 2D ROIs in specific axial slices (due to the time-intensive nature of such segmentation). Alternately, the automated segmentation could have included lesions, which were excluded by the expert reader during manual segmentation. Finally the manual segmentation was performed on single axial slices, which may have inadvertently excluded a region of the thalamus more affected by RRMS pathology. The quantitative pathology literature does not make such a distinction with the data, suggesting RRMS pathologic changes in the thalamus are randomly distributed although there are anecdotal comments that the anterior and medial nuclear groups may be more affected (Vercellino et al., 2009). A future study could prospectively attempt detailed, blinded, time-intensive manual thalamic parcellation to determine how specific thalamic nuclei are affected, and whether such T_2 changes correlate with clinical symptoms of fatigue, dystonia, memory impairment and reduced processing speed.

An advantage of the manual segmentation approach is the ability to sample specific white matter sub-regions, while automated FreeSurfer segmentation may include T_1 isointense, yet T_2 bright lesions, thereby confounding localized T_2 changes in normal-appearing regions. Hence, with this approach, EMC based T_2 values reflected subtle tissue changes for a variety of normal-appearing white matter structures in RRMS patients compared to healthy controls. Using manual regions-of-interest segmentations that excluded visible lesions on conventional T_2-weighted images, we observed small but significant increases in T_2 values for the corpus callosum in RRMS subjects (e.g. 11.4% increase in the body of the callosum, $p = 0.012$) (Table 2). In addition to changes in the T_2 value, we also observed consistent increases in T_2 *variance* for different brain regions in RRMS subjects compared to controls, suggesting higher heterogeneity in the underlying RRMS pathology burden. As expected, visible lesions on conventional MRI had T_2 values 35–39% higher than homologous white matter regions in healthy controls (all comparisons, $p < 0.001$) – this supports the external validity of this T_2 measurement technique, but was not the focus of the current study.

T_2 hyperintensity in obvious RRMS lesions can result from multiple concurrent changes in the local mesoscopic tissue environment, including inflammation, edema, blood-brain-barrier breakdown, abnormal remyelination, gliosis or axonal loss – it is difficult to attribute T_2 changes to a single specific microstructural pathologic change (Lund et al., 2012; MacKay et al., 2006). Besides these pathological changes, additional biophysical processes may also contribute to T_2 changes observed for normal-appearing brain tissue, including oligodendrocyte apoptosis with microglial activation (Barnett and Prineas, 2004), altered neuropil

Table 1
Mean, standard deviation (SD) and coefficient of variation (CV) of T_2 values in five brain regions for a single healthy volunteer. Values are calculated across the set of 24 scans used to test stability of EMC vs. Exponential fitting methods (see text for additional info). In addition to providing the correct T_2 value based on single spin echo reference (Ben-Eliezer et al., 2015a, 2015b), the EMC fitting algorithm produced lower SD and CV across all brain regions [WM: white matter; CC: corpus callosum].

ROI name	T_2 values: Mean ± SD [ms] (CV %)	
	EMC Fitting	Exponential fitting
Genu of CC	55.9 ± 2.1 (3.8)	87.6 ± 4.4 (5.0)
Splenium of CC	58.6 ± 2.7 (4.5)	93.8 ± 5.6 (6.0)
Caudate nucleus	56.0 ± 2.2 (4.0)	86.8 ± 5.5 (6.4)
Juxtacortical WM	53.0 ± 1.5 (2.9)	87.6 ± 3.7 (4.3)
Periventricular WM	63.5 ± 2.8 (4.3)	100.9 ± 3.6 (3.6)

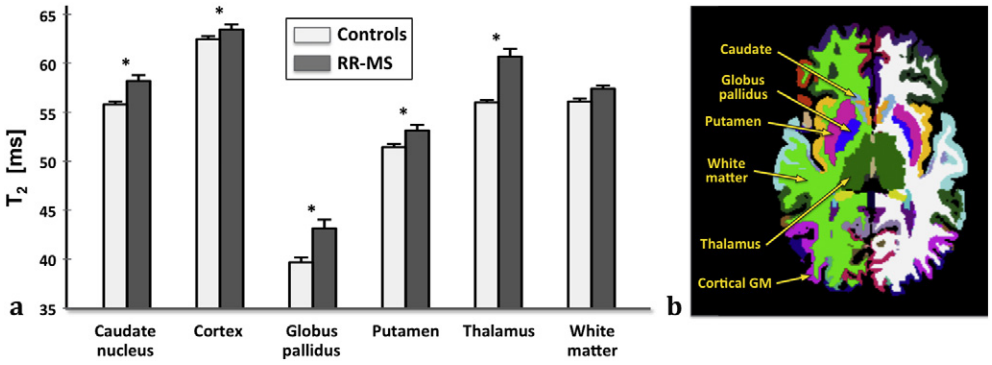

Fig. 3. (a) Bar graph comparing T_2 values (mean ± SD) in brain regions segmented using Freesurfer, in relapsing-remitting multiple sclerosis patients and in age-matched healthy controls (N = 27 & 38 subjects respectively). Regions that are statistically different between the two groups ($p < 0.05$) are denoted with "*". (b) Representative FreeSurfer segmentation map, overlaid on an axial T_1-weighted image at the level of the internal capsule.

(Moll et al., 2008), dysregulated iron deposition (Stankiewicz et al., 2007) and/or changes to myelination and reduced axonal diameter from prior tissue repair (Dula et al., 2010). The relative contributions of these pathologies may vary between individuals, anatomic regions and at different times during the natural history of RRMS. These results may justify future longitudinal studies in patients and radiology-pathology quantitative T_2 study in postmortem MS brains.

Several recent reports focused on multi-compartment T_2 fitting schemes to increase the pathologic specificity of T_2 relaxation measurements by correlating tissue histological changes to T_2-based estimations of myelin water fraction (MWF) (MacKay et al., 2006). Accordingly, MWF appears reduced 16% and water content increased 2% in normal-appearing white matter (Laule et al., 2004). However, MWF is challenging to estimate and lacks a gold-standard method that will provide stable and reliable values. Some potential confounds to calculating MWF include dependence on intercompartmental water exchange and on acquisition strategies (Dula et al., 2010; Harkins et al., 2012; Zhang et al., 2015a), or the failure to distinguish between intact myelin and myelin debris (Alonso-Ortiz et al., 2015). Magnetization transfer might also affect MWF calculation, although recent data suggests that this factor may not influence MSE-based MWF measurements (Zhang et al., 2015b). Our current data has not been subjected to this type of analysis, but it is our perspective that accurate T_2 estimation in RRMS patients with the EMC approach can eventually contribute to improved pathological specificity in particular brain regions or diseases. A limitation of the current EMC-derived single component T_2 fitting is that microstructural tissue pathologies that affect individual T_2 compartments independently, may be obscured or mitigate one another in a globally averaged measurement. The range of echo times used for data acquisition may also affect EMC estimation accuracy if very short and long T_2 components are intermixed in the same voxel.

4.2. Anatomic variation of T_2 in the healthy brain

Significant T_2 differences were observed between normal brain regions in the healthy control group. Mean T_2 values in the range of 70…90 ms for different brain regions (29% variance) beyond simple gray-white matter distinctions have been reported previously using

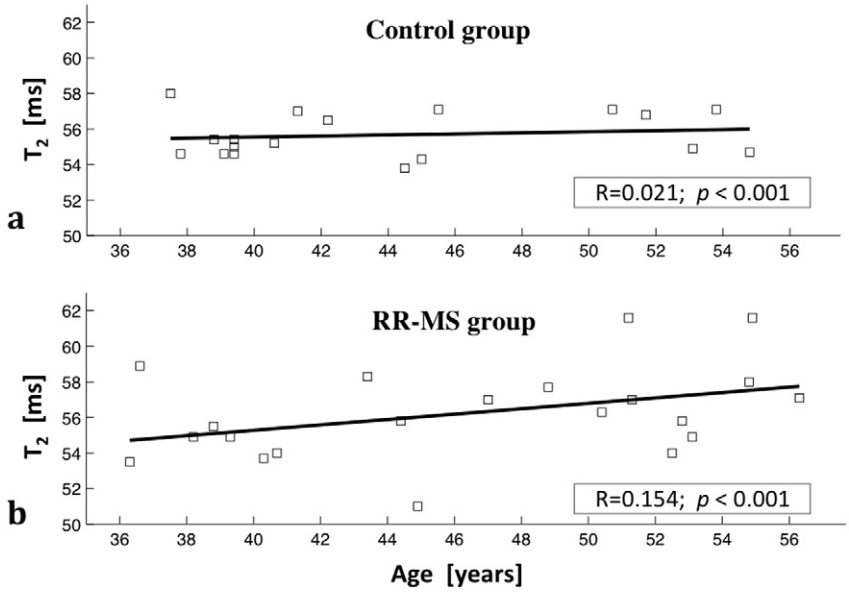

Fig. 4. Mean thalamic T_2 values using the manual segmentation were 8.5% higher in subjects with RRMS compared to age-matched healthy controls ($p < 0.001$). In controls, thalamic T_2 values were independent of subject age (a). T_2 values in RRMS patients showed minimal dependence on age (b).

Table 2
Summary of T_2 values from healthy controls and patients with relapsing-remitting multiple sclerosis (RR-MS) in different regions of the brain, manually segmented by expert neuroradiologist (mean ± SD). Statistically significant differences ($p < 0.05$) are highlighted in green.

Manually segmented ROI	Healthy controls [ms]	RR-MS patients [ms]	*t*-Test *p*-value
Optic radiations	52.3 ± 3.0	54.7 ± 3.8	0.609
Temporal stem	59.6 ± 2.1	62.6 ± 3.6	0.043
Globus pallidus	39.9 ± 3.7	40.0 ± 3.5	0.376
Caudate nucleus	57.1 ± 2.8	54.4 ± 3.7	0.069
Putamen	51.9 ± 1.9	51.7 ± 3.9	0.532
Thalamus	55.1 ± 1.7	57.0 ± 3.1	0.244
Posterior limb internal capsule	71.2 ± 3.5	68.8 ± 3.6	0.035
Genu corpus callosum	46.8 ± 2.3	48.8 ± 2.7	0.021
Splenium corpus callosum	55.3 ± 3.0	56.4 ± 3.0	0.84
Body corpus callosum	60.5 ± 4.4	67.6 ± 6.5	0.005
Centrum semiovale	61.0 ± 2.3	62.8 ± 2.8	0.703

exponential fits (Whittall et al., 1997). More recently, multiexponential T_2 values were shown to depend on estimated axon diameter, myelin thickness, and inter-compartmental exchange (Dula et al., 2010). Differences in T_2 mapping techniques and lack of gold standard prevent direct comparisons to our results, but support the observation that the variation in T_2 intrinsically depends on the underlying tissue mesoscopic structure. In healthy controls, EMC T_2 mapping demonstrated remarkably consistent differences amongst deep gray nuclei structures – for both automated and manual ROI analysis there was a 40% variation in T_2 values between globus pallidus and caudate nucleus (Table 2).

White matter T_2 values in healthy controls demonstrated spatial anatomic dependence (Fig. 5). In the cerebral hemispheres, T_2 values for periventricular, centrum semiovale, subcortical and juxtacortical white matter decreased in a centrifugal manner (mean T_2 decreasing 15% from 66.6 to 56.3 ms). A provocative result was that the T_2 of juxtacortical white matter in the hand knob of the precentral gyrus appeared significantly higher than other juxtacortical regions ($p < 0.0001$). Further, the posterior limb of the internal capsule demonstrated the highest white matter T_2 values (70.5 ± 3.9 ms) and was anecdotally noted to be brightest in the predicted location of the hand fibers for

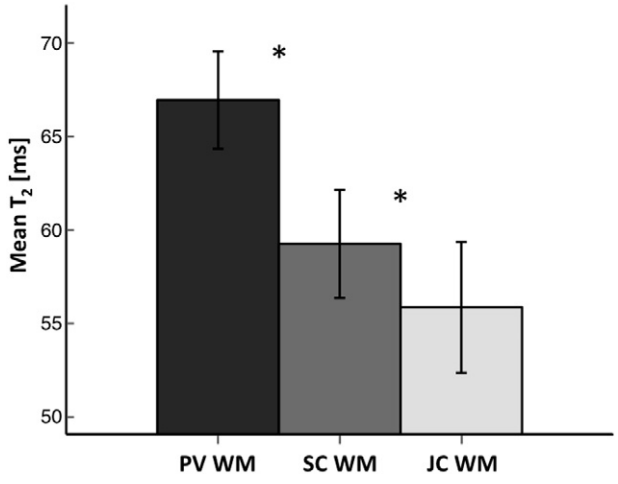

Fig. 5. Manual region-of-interest T_2 values (mean ± SD, N = 38) for periventricular (PV), subcortical (SC) and juxtacortical (JC) white matter (WM) regions in healthy controls decreased in a centrifugal manner (all three groups statistically different, $p < 0.05$). This trend may reflect different underlying mesoscopic tissue environments such as variations in axon caliber, dispersion, packing density, myelination or even orientation with respect to the MRI main magnetic field.

the corticospinal tract. Both these regions should include the corticospinal tract involved in the primary motor control of hand movements. Discordant T_2 decreases observed in the posterior limb internal capsule for RRMS patients (Table 2) might reflect a different tissue environment and requires further investigation. Similarly, T_2 for the genu, body and splenium of the corpus callosum, regions with different anatomic and functional connectivity, varied by 30% in healthy controls with all three regions statistically different (unpaired *t*-tests, $p < 0.0001$). Future studies could investigate whether T_2 is affected by callosal or internal capsule anatomic regional differences in bound water fraction, axon size, density, dispersion, myelination, and orientation relative to the main magnetic field (B_0). Accurate mapping of multiple T_2 components may be particularly informative for these interesting observations.

4.3. Validation of EMC based T_2 mapping

We have demonstrated the potential sensitivity of the novel EMC T_2 mapping technique in a large cohort of RRMS patients. The EMC algorithm offers more accurate T_2 mapping compared to conventional exponential fitting, which overestimated T_2 values by 30–100%. Perhaps more important, EMC based T_2 values are stable across different MRI scanners or acquisition protocols and does not have specific hardware requirements as recent advanced diffusion strategies (Ben-Eliezer et al., 2015b). Thus, it can be adapted to most existing MRI systems with multiecho acquisition capability. The variance amongst control subjects for individual regions was <5%. Further, the coefficient of variation was <4% for manual or automated ROI segmentation with repeat MRI scans in 3 healthy controls. Note that the EMC method differs substantially from previous T_2 mapping approaches yet has been thoroughly validated against single spin echo reference acquisitions (Ben-Eliezer et al., 2015a, 2016). These methodological differences limit our ability to make direct comparisons with previous results in the MS patient population.

5. Conclusions

We report the first application of the EMC quantitative T_2 mapping technique to RRMS patients. The current results demonstrate that this new method is stable and precise when applied to a large cohort of clinical subjects. We observed statistically significant T_2 increases in both normal-appearing white and gray matter structures for subjects with a clinically-established diagnosis of RRMS. Similar to diffusion, magnetization transfer, and spectroscopy (Ceccarelli et al., 2007; Davie et al., 1997; Mangia et al., 2014), the observed T_2 changes in normal-appearing tissues may reflect early neurodegeneration and/or chronic inflammatory myelin and glial pathology not visible to conventional MRI. In this initial case-control study, thalamic T_2 values alone demonstrated excellent discrimination of RRMS patients from controls (AUC = 0.913). We also observed interesting T_2 differences for different gray and white matter regions for healthy controls that may reflect functional and/or mesoscopic structural differences. Future prospective efforts will determine how region-specific T_2 quantification can be used to improve the diagnostic accuracy for early MS or distinguish MS subtypes, and determine whether regional brain T_2 quantification provide biomarkers for MS-associated clinical disability and disease progression.

Financial disclosure and declaration of interest

Timothy Shepherd received research support from the National Institute of Aging (NIH 1K23 AG048622-01). Ivan Kirov received research support from the National Institute of Neurological Disorders and Stroke (NIH R01 NS097494-01). This research was supported in part by the Center for Advanced Imaging Innovation and Research, an NIH NIBIB Biomedical Technology Resource Center (Grant P41EB017183). The authors have no other conflicts of interest to declare.

Appendix A. EMC fitting stability experiments

Stability of the EMC fitting algorithm was tested on a control subject recruited to undergo multiple MRI scans. Scans were performed using 6 different scan settings including slice thickness = 2, 3, and 4 mm, echo spacing = 10, 12, and 15 ms (equal to first echo time), and acquisition bandwidth = 200 and 399 Hz/Px. Each parameter-set was repeated twice, and on two different scanners (Trio and Skyra, Siemens Healthcare GmbH, Erlangen, Germany) to a total of 24 scans. The volunteer was taken out and back into the scanner between each consecutive scans without getting off the bed so as to minimize changes of the head orientation. Mean, standard-deviation (SD), and coefficient of variation (CV) were calculated for 5 ROIs selected from the larger group of ROIs in the MS subject study that were representative of different tissue environments in the brain: genu of corpus callosum, splenium of corpus callosum, right caudate nucleus, periventricular white matter, and subcortical white matter (GNU, SPL, CDN, PVWM, SCWM).

Inter-scanner variability was evaluated as the average difference between scans done on different scanners but with the same scan parameters. *Intra-scanner* variability was defined as the average SD within each ROI for scans performed on the same scanner but with different scan parameters. A third measure of stability, the *inter-subject* variability, was separately evaluated by collecting multi spin-echo T_2 mapping data for 38 healthy volunteers, ages [25…52] (15 females) in standard clinical setting (TR = 2500 ms, Echo-spacing = 12 ms, First echo-time = 12 ms, $N_{echoes} = 10$, res = 1.7×1.7 mm^2, slice thickness = 3 mm, bandwidth = 200 [Hz/Px], $T_{acquisition}$ = 2:44 min using 2× GRAPPA acceleration). Standard deviation of the T_2 values was subsequently calculated across the group for the abovementioned set of 5 ROIs. Lastly, a measure of *repeatability* was estimated for EMC and conventional exponential fitting by calculating the mean difference between the 6 identical pairs of scans. This was repeated for each of the 5 ROIs, producing a repeatability measure per ROI, which was then averaged to attain a global value per fitting method.

T_2 values for the 5 brain regions from repeated scans of a single subject yielded average *intra scanner* variability of 1.6 ms and 2.0 ms, and average *inter scanner* variability of 0.7 ms and 1.4 ms for the EMC and exponential fits respectively (Table A1). Average *inter subject* variability, measured across 38 healthy volunteers, was 2.5 and 4.3 ms for EMC and exponential fits respectively. While some variability can be attributed to slice misalignment between scans, these results suggest that EMC offers improved stability compared to exponential fitting in a large clinical cohort.

Table A1
Stability test results for the EMC vs. Exponential fitting. Columns 2–5: present inter- and intra-scanner variability of T_2 values for 5 brain ROIs of a single healthy volunteer, collected over a series of 24 separate scans (see text). Columns 6–7: inter subject variability of the mean T_2 values, estimated across a group of 38 healthy controls [EMC: EMC fitting; EXP: Exponential fitting].

ROI name	Intra-scanner variability [ms]		Inter-scanner variability [ms]		Inter-subject variability [ms]	
	EMP	EXP	EMP	EXP	EMC	EXP
Genu of CC	1.5	1.5	0.6	1.1	2.3	3.9
Splenium of CC	1.4	1.7	0.6	1.1	3.0	5.7
Caudate nucleus	1.6	2.2	1.0	2.8	2.8	5.1
Juxtacortical WM	2.0	2.2	0.6	0.8	2.0	3.1
Periventricular WM	1.5	2.4	0.7	1.0	2.3	3.5
Average variability	**1.6**	**2.0**	**0.7**	**1.4**	**2.5**	**4.3**

Appendix B. Supplementary data

Supplementary data to this article can be found online at http://dx.doi.org/10.1016/j.nicl.2017.01.029.

References

Alonso-Ortiz, E., Levesque, I.R., Pike, G.B., 2015. MRI-based myelin water imaging: a technical review. Magn. Reson. Med. 73 (1):70–81. http://dx.doi.org/10.1002/mrm.25198.

Barkhof, F., 2002. The clinico-radiological paradox in multiple sclerosis revisited. Curr. Opin. Neurol. 15 (3), 239–245.

Barnett, M.H., Prineas, J.W., 2004. Relapsing and remitting multiple sclerosis: pathology of the newly forming lesion. Ann. Neurol. 55 (4), 458–468.

Ben-Eliezer, N., Sodickson, D.K., Block, K.T., 2015a. Rapid and accurate T2 mapping from multi-spin-echo data using Bloch-simulation-based reconstruction. Magn. Reson. Med. 73 (2), 809–817.

Ben-Eliezer, N., Cosi, V., Yoshimoto, E.A., Sodickson, D.K., Bruno, M., Block, K.T., Shepherd, T., 2015b. Identification of quantitative differences in normal-appearing white matter of multiple sclerotic patients vs. healthy controls using a novel Bloch-simulation-based T2 mapping technique. Proc. Int. Soc. Magn. Reson. Med. 23, 4364 (unpublished material available as supplementary material).

Ben-Eliezer, N., Sodickson, D.K., Shepherd, T., Wiggins, G.C., Block, K.T., 2016. Accelerated and motion-robust in vivo T2 mapping from radially undersampled data using bloch-simulation-based iterative reconstruction. Magn. Reson. Med. 75 (3), 1346–1354.

Bonnier, G., Roche, A., Romascano, D., Simioni, S., Meskaldji, D., Rotzinger, D., Lin, Y.C., Menegaz, G., Schluep, M., Pasquier, R.D., Sumpf, T.J., Frahm, J., Thiran, J.P., Krueger, G., Granziera, C., 2014. Advanced MRI unravels the nature of tissue alterations in early multiple sclerosis. Ann. Clin. Transl. Neurol. 1 (6):423–432. http://dx.doi.org/10.1002/acn3.68.

Ceccarelli, A., Rocca, M.A., Falini, A., Tortorella, P., Pagani, E., Rodegher, M., Comi, G., Scotti, G., Filippi, M., 2007. Normal-appearing white and grey matter damage in MS. A volumetric and diffusion tensor MRI study at 3.0 Tesla. J. Neurol. 254 (4), 513–518.

Davie, C.A., Barker, G.J., Thompson, A.J., Tofts, P.S., McDonald, W.I., Miller, D.H., 1997. 1H magnetic resonance spectroscopy of chronic cerebral white matter lesions and normal appearing white matter in multiple sclerosis. J. Neurol. Neurosurg. Psychiatry 63 (6), 736–742.

Deoni, S., Rutt, B., Peters, T., 2003. Rapid combined T1 and T2 mapping using gradient recalled acquisition in the steady state. Magn. Reson. Med. 49 (3), 515–526.

Dula, A.N., Gochberg, D.F., Valentine, H.L., Valentine, W.M., Does, M.D., 2010. Multiexponential T2, magnetization transfer, and quantitative histology in white matter tracts of rat spinal cord. Magn. Reson. Med. 63 (4):902–909. http://dx.doi.org/10.1002/mrm.22267.

Gilmore, C.P., Donaldson, I., Bö, L., Owens, T., Lowe, J., Evangelou, N., 2009. Regional variations in the extent and pattern of grey matter demyelination in multiple sclerosis: a comparison between the cerebral cortex, cerebellar cortex, deep grey matter nuclei and the spinal cord. J. Neurol. Neurosurg. Psychiatry 80 (2):182–187. http://dx.doi.org/10.1136/jnnp.2008.148767.

Harkins, K.D., Dula, A.N., Does, M.D., 2012. Effect of intercompartmental water exchange on the apparent myelin water fraction in multiexponential T2 measurements of rat spinal cord. Magn. Reson. Med. 67 (3):793–800. http://dx.doi.org/10.1002/mrm.23053.

Hohol, M.J., Orav, E.J., Weiner, H.L., 1995. Disease steps in multiple sclerosis: a simple approach to evaluate disease progression. Neurology 45 (2), 251–255.

Huang, C., Bilgin, A., Barr, T., Altbach, M., 2012. T2 relaxometry with indirect echo compensation from highly undersampled data. Magn. Reson. Med. 70 (4), 1026–1037.

Khalil, M., Enzinger, C., Langkammer, C., Tscherner, M., Wallner-Blazek, M., Jehna, M., Ropele, S., Fuchs, S., Fazekas, F., 2009. Quantitative assessment of brain iron by R(2)* relaxometry in patients with clinically isolated syndrome and relapsing-remitting multiple sclerosis. Mult. Scler. 15 (9):1048–1054. http://dx.doi.org/10.1177/1352458509106609.

Laule, C., Vavasour, I.M., Moore, G.R.W., Oger, J., Li, D.K.B., Paty, D.W., MacKay, A.L., 2004. Water content and myelin water fraction in multiple sclerosis - a T2 relaxation study. J. Neurol. 251:284–293. http://dx.doi.org/10.1007/s00415-004-0306-6.

Laule, C., Vavasour, I.M., Leung, E., Li, D.K., Kozlowski, P., Traboulsee, A.L., Oger, J., Mackay, A.L., Moore, G.R., 2011. Pathological basis of diffusely abnormal white matter: insights from magnetic resonance imaging and histology. Mult. Scler. 17 (2):144–150. http://dx.doi.org/10.1177/1352458510384008.

Laule, C., Pavlova, V., Leung, E., Zhao, G., MacKay, A.L., Kozlowski, P., Traboulsee, A.L., Li, D.K., Moore, G.R., 2013. Diffusely abnormal white matter in multiple sclerosis: further histologic studies provide evidence for a primary lipid abnormality with neurodegeneration. J. Neuropathol. Exp. Neurol. 72 (1):42–52. http://dx.doi.org/10.1097/NEN.0b013e31827bced3.

Learmonth, Y.C., Motl, R.W., Sandroff, B.M., Pula, J.H., Cadavid, D., 2013. Validation of patient determined disease steps (PDDS) scale scores in persons with multiple sclerosis. BMC Neurol. 13:37. http://dx.doi.org/10.1186/1471-2377-13-37.

Lebel, R., Wilman, A., 2010. Transverse relaxometry with stimulated echo compensation. Magn. Reson. Med. 64 (4), 1005–1014.
Levitt, M.H., 2001. Spin Dynamics: Basics of Nuclear Magnetic Resonance. Wiley (ISBN 978-0-471-48922-1).
Liu, S., Kullnat, J., Bourdette, D., Simon, J., Kraemer, D.F., Murchison, C., Hamilton, B.E., 2013. Prevalence of brain magnetic resonance imaging meeting Barkhof and McDonald criteria for dissemination in space among headache patients. Mult. Scler. J. 19 (8), 1101–1105.
Lukzen, N., Petrova, M., Koptyug, I., Savelov, A., Sagdeev, R., 2009. The generating functions formalism for the analysis of spin response to the periodic trains of RF pulses. Echo sequences with arbitrary refocusing angles and resonance offsets. J. Magn. Reson. 196 (2), 164–169.
Lund, H., Jønsson, A., Andresen, J., Rostrup, E., Paulson, O.B., Sørensen, P.S., 2012. Cognitive deficits in multiple sclerosis: correlations with T2 changes in normal appearing brain tissue. Acta Neurol. Scand. 125 (5):338–344. http://dx.doi.org/10.1111/j.1600-0404.2011.01574.x.
Ma, D., Gulani, V., Seiberlich, N., Liu, K., Sunshine, J., Duerk, J., Griswold, M., 2013. Magnetic resonance fingerprinting. Nature 14 (495(7440)), 187–192.
MacKay, A., Laule, C., Vavasour, I., Bjarnason, T., Kolind, S., Mädler, B., 2006. Insights into brain microstructure from the T2 distribution. Magn. Reson. Imaging 24 (4), 515–525.
Mangia, S., Carpenter, A.F., Tyan, A.E., Eberly, L.E., Garwood, M., Michaeli, S., 2014. Magnetization transfer and adiabatic T1ρ MRI reveal abnormalities in normal-appearing white matter of subjects with multiple sclerosis. Mult. Scler. 20 (8):1066–1073. http://dx.doi.org/10.1177/1352458513515084.
McPhee, K.C., Wilman, A.H., 2016. Transverse relaxation and flip angle mapping: evaluation of simultaneous and independent methods using multiple spin echoes. Magn. Reson. Med. http://dx.doi.org/10.1002/mrm.26285.
Minagar, A., Barnett, M.H., Benedict, R.H., Pelletier, D., Pirko, I., Sahraian, M.A., Frohman, E., Zivadinov, R., 2013. The thalamus and multiple sclerosis: modern views on pathologic, imaging, and clinical aspects. Neurology 80 (2):210–219. http://dx.doi.org/10.1212/WNL.0b013e31827b910b.
Moll, N.M., Rietsch, A.M., Ransohoff, A.J., Cossoy, M.B., Huang, D., Eichler, F.S., Trapp, B.D., Ransohoff, R.M., 2008. Cortical demyelination in PML and MS: similarities and differences. Neurology 70 (5), 336–343.
Polman, C.H., et al., 2010. Diagnostic criteria for multiple sclerosis: 2010 revisions to the McDonald criteria. Ann. Neurol. 69 (2):292–302. http://dx.doi.org/10.1002/ana.22366.
Poon, C.S., Henkelman, R.M., 1992. Practical T2 quantification for clinical application. J. Magn. Reson. Imaging 2 (5):541–553. http://dx.doi.org/10.1002/jmri.1880020512.
Prasloski, T., Mädler, B., Xiang, Q., MacKay, A., Jones, C., 2012. Applications of stimulated echo correction to multicomponent T2 analysis. Magn. Reson. Med. 67 (6), 1803–1814.
Schmitt, P., Griswold, M., Jakob, P., Kotas, M., Gulani, V., Flentje, M., Haase, A., 2004. Inversion recovery TrueFISP: quantification of T(1), T(2), and spin density. Magn. Reson. Med. 51 (4), 661–667.
Stankiewicz, J., Panter, S.S., Neema, M., Arora, A., Batt, C.E., Bakshi, R., 2007. Iron in chronic brain disorders: imaging and neurotherapeutic implications. Neurotherapeutics 4 (3), 371–386.
Sussman, M.S., Vidarsson, L., Pauly, J.M., Cheng, H.L., 2010. A technique for rapid single-echo spin-echo T2 mapping. Magn. Reson. Med. 64 (2):536–545. http://dx.doi.org/10.1002/mrm.22454.
Vercellino, M., Masera, S., Lorenzatti, M., Condello, C., Merola, A., Mattioda, A., Tribolo, A., Capello, E., Mancardi, G.L., Mutani, R., Giordana, M.T., Cavalla, P., 2009. Demyelination, inflammation, and neurodegeneration in multiple sclerosis deep gray matter. J. Neuropathol. Exp. Neurol. 68 (5):489–502. http://dx.doi.org/10.1097/NEN.0b013e3181a19a5a.
Warntjes, J., Dahlqvist, O., Lundberg, P., 2007. Novel method for rapid, simultaneous T1, T*2, and proton density quantification. Magn. Reson. Med. 57 (3), 528–537.
Whittall, K.P., MacKay, A.L., Graeb, D.A., Nugent, R.A., Li, D.K., Paty, D.W., 1997. In vivo measurement of T2 distributions and water contents in normal human brain. Magn. Reson. Med. 37 (1), 34–43.
Zhang, J., Kolind, S.H., Laule, C., MacKay, A.L., 2015a. Comparison of myelin water fraction from multiecho T2 decay curve and steady-state methods. Magn. Reson. Med. 73 (1):223–232. http://dx.doi.org/10.1002/mrm.25125.
Zhang, J., Kolind, S.H., Laule, C., MacKay, A.L., 2015b. How does magnetization transfer influence mcDESPOT results? Magn. Reson. Med. 74 (5):1327–1335. http://dx.doi.org/10.1002/mrm.25520.